Journal of Materials Chemistry C

Tunable wide blue photoluminescence with europium decorated graphene

Journal:	*Journal of Materials Chemistry C*
Manuscript ID:	TC-ART-10-2014-002361.R2
Article Type:	Paper
Date Submitted by the Author:	10-Feb-2015

Complete List of Authors:	Park, Byeongho; Yonsei University, Mechanical Engineering Kim, Sun Jun; Yonsei University, Mechanical Engineering Lim, juhwan; Yonsei University, Mechanical Engineering Some, Surajit; Yonsei University, Mechanical Engineering; Institute of Chemical Technology, Department of Dyestuff Technology Park, Ji-eun; Ewha Womans University, Chemistry & Nano Science Kim, Sung-Jin; Ewha Womans University, Division of Nano Sciences Kim, Chulki; Korea Institute of Science and Technology (KIST), Sensor System Research Center Lee, Taikjin; Korea Institute of Science and Technology (KIST), Sensor System Research Center Jun, Seong Chan; Yonsei University, Mechanical Engineering

Tunable wide blue photoluminescence with europium decorated graphene

Byeongho Park[a], Sun Jun Kim[a], Juhwan Lim[a], Surajit Some[b], Ji-eun Park[c], Sung-jin Kim[c], Chulki Kim[d], Taikjin Lee[d] and Seong Chan Jun[a,*]

a: NEMD Lab, Department of Mechanical Engineering, Yonsei University, Seoul 120-749, South Korea

b: Department of Dyestuff Technology, Institute of Chemical Technology, Matunga, Mumbai-400 019, India

c: Department of Chemistry and Nano Science, Ewha Woman's University, Seoul 120-750, South Korea

d: Sensor System Research Center, Korea Institute of Science and Technology (KIST), Seoul, South Korea

*: The person to whom correspondence, scj@yonsei.ac.kr, Tel: +82-2-2123-5817; Fax: +82-2-312-2159

Abstract

The current paper describes europium decorated graphene (EuG) provides high and wide blue emission at 400 nm and 458 nm. The chemical and structural properties of the products are characterized by X-ray photoelectron spectroscopy (XPS), X-ray diffraction (XRD), Raman spectroscopy and transmission electron microscopy. Fourier transform infrared (FT-IR) and UV-Vis spectrometers are employed to analyze the optical property. Photoluminescence features are investigated by excitation/emission spectrum and fluorescence microscopy image. The photoluminescence intensity of EuG with the bright fluorescent nature in europium is higher than that of reduced graphene oxide. The transition of trivalent europium (Eu^{3+}) that lead to radiate the light with 590 nm of wavelength can be turned into a 4*f*-4*f* transition of divalent (Eu^{2+}) europium upon heating in the presence of graphene sheet, which assists the reduction of the europium ion. The enhancement of the blue emission at 458 nm with quenching in the red at 590 nm is effected by modified property from europium-graphene composite concentration and external thermal energy. The result suggests a new possibility for fluorescent characteristics of lanthanide-graphene nanocomposite that can be applied to display, optoelectronic devices, and bio-imaging fields.

The tunable photoluminescence characteristics by temperature can be used as a non-contact thermal sensor.

Keywords : Annealing, blue emission, europium, graphene, photoluminescence

Introduction

Graphene sheet **-** an sp^2 carbon bonding-based two-dimensional structure with single-atom thickness **-** has attracted attention with its promising physical and electrical properties such as high elasticity, quantum electronic transport and excellent high mobility due to its unique band gap structure. [1-3] These fascinating properties suggest potential applications in various technological fields including nanocomposites, [4] nanoelectronics, [5-7] optoelectronics [8, 9] and supercapacitors. [10-12] Particularly, fluorescence of graphene have intensely studied for bandgap research and emission spectrum investigation, since the electrical and mechanical property of graphene with atomic size thin film structure is significantly appropriate to optoelectrical device and bio-imaging sytem in nanoscale. However, the properties of graphene are considerably sensitive to its intrinsic atomic structure and external modifications such as annealing [13] or chemical treatments [14]. For example, closed band gap of monolayer graphene [15] can be opened as the number of layers increased. Graphene oxide (GO), which can change its chemical structure from different treatment, exposed a new opening to control the band structure of graphene-based material. Especially, the presence of numerous functional groups on the graphene oxide surface provides the potential for use in nanocomposites. There are a number of report of GO-based-nanocomposites with several metal ions such as copper, [16] palladium, [14, 17] titanium, [18] platinum [19] and gold nanoparticles. [20, 21] Also, current study introduced GO decorated with other materials including polymers, [22] and hydrogels. [23]

Lanthanide atoms such as Er, Yb, Ce, and Eu are outstanding candidates for compound

with graphene. $NaYF_4:Er^{3+}/Yb^{3+}$–graphene composites provides bright green upconversion emissions and it reveals a capability for applying to the solar cell. [24] Cerium dioxide complexed graphite oxide and graphene, which shows the thermal stability and the electrochemistry sensor ability, were synthesized by hydrothermal reduction. [25] Europium is a well-known material that has a fluorescent emission near a wavelength of 600 nm due to the $^5D_0 \rightarrow {}^7F_{J\ (J=1,\ 2,\ 3,\ 4,\ 5)}$ transition assisted with, for instance, carbon nanotubes, [26] titania [27] and metal nanoparticles. Graphene-europium complex has bifunctional characteristics, i.e., luminescence and quenching capabilities. [28] Furthermore, europium showed not only red emission feature but also the blue emission with its efficient fluorescence. [29, 30]

In this paper, we showed the tunable broad blue emission of europium decorated graphene (EuG) with different europium concentrations using simple thermal annealing method. The results of this study suggests one of the capable resources for graphene-based blue fluorescent material that allows various optoelectrical applications.

1. Experimental

Composites of ultrasmall Eu_2O_3 nanoparticles [31] and GO, produced by an improved Hummers method, [32, 33] were synthesized by adding GO (0.10 g) and $Eu(NO_3)_3{\cdot}6H_2O$ at four different weight percents, 0.05, 0.5, 1, and 50 wt%, relative to the quantity of GO. Appropriate amounts of Eu_2O_3 and GO were added to triethylene glycol (30 mL) in a flask and stirred at 50 ºC until the reaction was complete. Then, NaOH (0.035g) was added and the mixture was heated to 80 ºC. Lastly, a H_2O_2 (0.4425mL) aqueous solution was slowly introduced at 80 ºC over an additional 2 hours.

The film samples for annealing were prepared on a quartz substrate, which is transparent in the visible range with 1 cm by 1 cm area and a 1 mm thickness. Samples were prepared by

repeated spin coating with 300, 500, 800, 1600 rpm for 40 s each, totally 160 s. A furnace was employed to heat the EuG samples at different temperatures from 400 ℃ to 1000 ℃ in an argon atmosphere. We used transmission electron microscopy (TEM) (JEOL, FE-TEM) and Cs-corrected spherical aberration correction scanning transmission electron microscope (JEOL, JEM-ARM 200F) to illustrate the structures and surfaces of samples with high resoluion (~0.1nm). The luminescence graphene with europium was analyzed using X-ray photoemission spectroscopy (XPS) (VG Scientific Instruments, ESCALAB 220i-XL), X-ray diffraction (XRD) measurements (RIGAKU, Ultima IV), Raman spectroscopy (Renishaw, InVia Micro Raman spectroscope excitation at 532 nm) and Fourier transform infrared (FT-IR) spectrum (Bruker, Vertex70). Absorbance spectrum was measured from UV/VIS spectrophotometer(JASCO Corporation, V-650). Photoluminescence (PL) of the EuG film samples was investigated using a fluorescence spectrophotometer (PerkinElmer, LS-55) and fluorescence microscope (Olympus, IX 71 (IX2 series)).

2. Results and Discussion

Figure 1 shows the morphology of typical single, thin layer graphene composites observed by high resolution TEM, which monitored EuG samples with different europium weight percent from 0.05 wt% to 50 wt%. The black spots representing Eu_2O_3 nanoparticles (3-10 nm) (Figure S1) were homogeneously distributed on the graphene sheet without aggregation in the image of the sample composed 0.05 wt% and 0.5 wt% europium (Figure 1(a),(b)), and some aggregated particles were revealed in the sample with europium concentration of 1 wt% and 50 wt% (Figure 1(c),(d)). In the Figure 1(a) and (b), the crystalline structure of graphene and europium is represented with fast Fourier transform (FFT) pattern in the observed region. Our EuG provides typical atomic thin structure of graphene with the hexagonal graphene lattice and europium-graphene complex area with different lattice form similar as reported

study. [28] As the weight percent of europium in the EuG increased from 0.05 wt% to 50 wt%, the number of spots as the europium nanoparticles also increased. At 50 wt%, the europium oxide fully covered the graphene sheet surface, as observed in Figure 1(d). The europium particle attached onto the graphene sheet leads to vary the crystalline structure as a defect. TEM image of EuG samples shows the graphene sheet and europium composite nanoparticles on the surface, which is different with europium-complexed graphene composed of atomic bonding between one europium atom and carbon sheet studied in the previous work. [28]

There are various functionalities in EuG, illustrated by the several XPS spectral peaks shown in Figure 2. Curve fitting of the C1s XPS spectra, represented in Figure 2 using a Gaussian-Lorentzian peak shape, were used to obtain specific information related to atomic bonding. The mean square error between well-known peaks and experimental data was minimized to confirm the fit. Figures 2(a)-(d) show the XPS spectra of the C1s orbital in EuG samples with different europium nanoparticle weight percent from 0.05 wt% to 50 wt% after annealing. The C1s XPS spectra of the EuG film demonstrate the degree of oxidation with several atomic bondings: C–C and C–H bonding at 284.5–285 eV, C–OH/ C–O–C at 286–286.5 eV, and O–C–OH at 289.3 eV. [34, 35] All samples have a peak located at 284.6 eV due to C–C and C=C bonding. The dominant bonding type in a typical carbon-based material is sp^2 due to the atomic-scale honeycomb lattice made of carbon atoms in graphene. The 0.05 wt% EuG, as shown in Figure 2(a), had a higher peak of C=O bonding located at 286.5 eV than did the 50 wt% EuG, as shown in Figure 2(d). This is because europium assisted the bonding between carbon and epoxy groups during formation of the composite. Before annealing for reduction of the sample, the C1s XPS spectrum showed that the EuG films had various functional groups composed of sp^2 clusters of several sizes and randomly spread sp^3 sites related to the disorder and a tunnel barrier among the clusters. Figures 2(a)-(d) show a

gradual decline in the sp^3 carbon and oxygen bonding due to annealing. The increase in the relative peak intensity at 284.6 eV indicates that the sp^2 clusters increased during annealing in an Ar atmosphere. [35] In contrast, there was a clear trend of decreasing intensity in the peaks at 286–286.5 eV and 289.3 eV, which are related to C–OH/ C–O–C and O–C–OH bonding, respectively. EuG samples undergo reduction by annealing, resulting in slightly decreased sp^3 sites, while the europium influences the peaks generated by the bonding between carbon and other atoms such as oxygen and europium. Thus, all of the relative peak intensities located between 286.5 eV and 289.3 eV were higher for EuG samples after heating than those of a pure reduced GO sheet. [34] Finally, a change in peak intensity was revealed for annealing until 1000 ºC because it was known that the GO is reduced fully at 850 ºC. [36]

The results shown in Figures 2(e)-(h) show Eu3d XPS spectra peaks located at 1125 eV, 1134 eV, 1156eV and 1165 eV, which are evidence of the atomic bonding with europium. [37-39] Europium atoms formed bonds with carbon and oxygen in the all of samples, based on the XPS spectra results in Figure 2. The prominent peaks around 1134 eV and 1165 eV with different spin-orbit components for the 5/2 and 3/2, respectively, indicate the presence of Eu^{3+} ($3d4f^6$). Moreover, we assigned the other small peaks at 1125 eV to a $Eu^{2+}_{5/2}$ ($3d4f^7$) configuration and at 1156 eV to $Eu^{2+}_{3/2}$. [27] The XPS features of Eu^{2+} and Eu^{3+} occur together for several reasons such as surface valence transitions and the presence of mixed trivalents. [27]

In Figure 2(e), the XPS spectra results for 0.05 wt% EuG annealed at 1000 ºC show that the intensity of the europium divalent peaks located at 1125 eV and 1156 eV were relatively higher than those of other experiments carried out at different temperatures, since the bonding with europium divalent increased. Graphene sheet assisted reduction of europium during annealing and the Eu^{3+} configuration significantly changed to the Eu^{2+} configuration. For 0.5 wt%, 1 wt%, and 50 wt% EuG, there was only a small difference in the Eu3d XPS spectra

during annealing until 1000 ºC, as shown in Figures 2(f)-(h). This is because the europium was present at sufficient concentration to bond with most of functional groups on graphene and adequately bonded europium and graphene lead to maintain its state. In Figure S2, O1s XPS spectrum was changed by thermal reduction according to heating temperature and concentration of europium. For 0.05 wt% and 1 wt% (Figure S2(a), (b)), there were considerable XPS spectrum change of europium and oxygen bonding located at 529, 531.4 eV after annealing at 1000 ºC. [40] For 1 wt% and 50 wt% (Figure S2(c), (d)), there were shifting of O1s XPS peak from 532.2 eV to 533.8 eV with reduction of graphene sheet.

XRD patterns of the EuG samples with different weight percent of europium and different annealing temperatures are presented in Figure 3. It is apparent from the XRD peaks at $2\theta \approx$ 23-26° that the graphene played a key role in changing the phase and surface structure, which determine the physical properties. [41, 42] Moreover, the full width at half maximum (FWHM) values of XRD peaks were larger than those of usual reduced graphene oxide since the samples had heterogeneous compositions of $Eu(OH)_3$, Eu_2O_3, and the complex of europium and graphene. [26] As the annealing temperature increased to 800 ºC, the XRD peaks shrank and shifted, which indicates that the inter layer distance between the graphene sheets was significantly reduced. [13] This occurred because carboxyl groups (-COOH) and hydroxyl groups (C-OH and O-H) were gradually removed by heating. The sharpest XRD peaks in 0.05 wt% and 0.5 wt% EuG were observed at 600 ºC; however, in the 1 wt% and 50 wt% EuG, the sharpest peak was observed at 800 ºC due to the effect of europium oxide reduction. Europium contributes to the XRD features, as shown in Figure 3. The 0.05 wt% EuG annealed at 400 ºC had a peak at 23.6°, which indicates amorphous-like carbon containing many defects, folding structures, impurities, and sp^1, sp^2, and sp^3 hybridization structures. In this study, the impurities and sp^3 orbital bonding contributed considerably to the peak at 23.6°.

[13, 43] After annealing at 400 ºC to remove H_2O and invaded gases, 0.5 wt% EuG had two peaks at 22.5° and 25°. The first peak at 22.5° is closely related with reduced graphene oxide, which is similar to that of the 0.05 wt% EuG sample, and the second peak at 25° arose from europium-substituted bonding. [26] As the weight percent of europium in EuG increased, the XRD features shifted, due to the increase amount of europium. The diffraction lines and (222) and (400) crystal planes of typical europium oxide are strongly represented in Figure 3(d) due to the coverage increment of europium on the graphene sheet surface with high concentration as shown in TEM image. [44]

In Figure 4, Raman shift spectra were analyzed with the samples reduced by thermal annealing based on the ratio of D- and G-band intensity and FWHM of peaks, respectively. The D-band near 1350 cm^{-1} indicates phonon vibrations related to the sp^3 orbital associated with the oxygen functionalities, i.e., defect-induced elastic scattering. The G-band near 1598 cm^{-1} represents the effect of the bonding including conjugated and single bonding with sp^2 orbitals in carbon-based materials. [34, 45] EuG has D and G-band peaks similar to those of GO. The ratio of intensity between the D- and G-band (I_D/I_G) indicates the degree of disorder in carbon-based material and the size of the sp^2 domains. In Figures 4(e)-(h), intrinsic EuG of 0.05, 0.5, 1, 50 wt% have I_D/I_G ratios of 0.934, 0.897, 1.062, and 0.995, respectively. The D/G ratios of EuG samples were varied differently with that of typical GO since the europium play a role in an impurity in the structure and europium could interact with both carbon and oxide. EuG of 50 wt%, which the graphene surface is fully covered by Eu, as shown in TEM image (Figure 1(d)), provides decrease of I_D/I_G ratio than other EuG with lower concentration of Eu. As annealing temperature increased, the ratio of intensities changed with the reduction of the sample.

The results of Raman shift spectra show a small change in the range of 600-800 ºC since

carbon in the CO and CO_2 gas were generated from disordered carbon positioned at the edges and boundaries of empty spaces in the graphene sheets. I_D/I_G increased to 1.141, 1.130, 1.086 and 1.031, respectively, for 0.05, 0.5, 1, 50 wt% EuG samples after annealing at 1000 ºC. This indicates that the degree of disorder in the material increased after heating due to bond fracture, which then simultaneously severed adjacent C=C aromatic bonds. [36] The I_D/I_G of 0.05 and 0.5 wt% EuG increased more drastically than that of 1 and 50 wt% EuG during annealing from room temperature to 1000 ºC. The 0.05 and 0.5 wt% EuG showed a much stronger combination effect (synergetic effect) by constructing the composite with a large change in I_D/I_G after annealing than did the 1 and 50 wt% EuG. The I_D/I_G ratio changed randomly in the 1 and 50 wt% EuG according to heating temperature, as shown in the Figures 4(g) and (h), since the state change of high concentration europium and graphene sheet by thermal energy generated arbitrary disorder in the materials with various functional groups. In Figures 4(i)-(l), the FWHM of the G-band, which describes the sharpness of the peak, indicates that the crystallinity of graphene was enhanced; this is declined by the thermal annealing effect at 1000 ºC. It is consistent results with XPS and XRD in terms of full reduction annealing temperature near 850 ºC.

FT-IR spectra of all of samples were analyzed for the compositional and structural property as shown in Figure 5. The EuG samples provided absorption bands located at 1050 cm^{-1} which indicates the C-O vibration, and at 1237 cm^{-1} corresponding to the C-OH vibration and around 1580 cm^{-1} to –COOH group vibrations. [14, 46] The characteristic bands at 1728 cm^{-1} of the C=O stretching vibrations from carbonyl and carboxylic groups was also revealed. And Eu-O vibrations of the bands at 415 cm^{-1}, 687 cm^{-1} and 779 cm^{-1} were represented. [46] After annealing EuG samples, C-O, C-OH, -COOH bands were drastically decreased with thermal reduction and Eu-O vibrations were enhanced with state change of material. The band around

3400 cm^{-1} assigned to the stretching and deformation vibration of OH and increased by heat energy. In the 50 wt% EuG with Figure 1(d), the smallest C-OH band was observed since the europium oxide covered considerably large area.

To analyze the absorption charateristics, UV/Vis spectrometer was employed with EuG samples as represented in Figure 6. EuG samples shows two absorption peaks located near 240 nm and 400 nm, these peaks were shifted with thermal reduction to the longer wavelength. Due to the π-π* transition between carbons in the different size of graphene sheet, usual graphene based composites provides the absorption feature near 240 nm and the reduction effect on the change of optical property with red-shift of peak from 240 to 258 nm. [14, 47] The second absorption peak at 400 nm is produced by defect levels in the EuG sample. In the 0.05, 0.5, 1 wt% EuG, the peak near 240 nm is higher than the second peak at 400 nm while the two peaks of 50 wt% EuG provides similar absorbance because the graphene sheet area of 50 wt% EuG is much smaller than other samples.

The photoluminescence excitation (PLE) of EuG samples was investigated by fluorescence spectrophotometer at the 458 nm of emission wavelength (Figure S3). The PLE peaks are revealed near 260 nm, specifically 0.05 wt% of EuG provides the highest intensity and PLE peak located at 258 nm. As increasing the concentration of europium in EuG from 0.05 to 50 wt%, the PLE peak positions slightly shift to longer wavelength sequentially. These peak position shift and intensity changes according to quantity of europium in EuG allow to control the photoluminescence characteristics. In the fully annealed 50 wt% EuG, the PLE spectrum shows different spectra, high-intensity band from 250 nm to 259 nm, with other PLE results. The thermal reduction of EuG contributes to enhance the PLE peak near 258 nm as increasing temperature. Modification technique of PL is one of the interesting issues of fluorescence graphene research. Using the fluorinated graphene, tunable photoluminescence

material was studied with hydroxylation developed in the previous research.[48] Furthermore, the EuG PLE near 260 nm can be used for near-infrared upconversion, which is usually utilized for solar cells. Nanoparticle based upconversion materials were reported such as $NaGd(WO_4)_2$ with Tm^{3+} which can be applied to the dye-sensitized solar cells. [49]

PL of the europium-complexed graphene with doping effect was investigated in the red emission and the quenching effect assisted by graphene sheet. [28] In this study, EuG composed of europium nanoparticles with annealing for thermal reduction provides the controllable blue emission. The EuG PL emission spectra of excitation at 258 nm by a UV light source are presented in Figure 7. Photons at 258 nm (4.8eV) have enough energy to excite electrons from the ground state to the $4f^{n-1}5d$ configuration. The peak near 400 nm, which represents the luminescent characteristic of graphene oxide with sp^3 bonding between carbon and oxygen, is dominant, [50, 51] and europium provides PL emission characteristics of the intrashell transition $^5D_0 \rightarrow {}^7F_J$ (J=0, 1, 2, 3, 4) of Eu^{3+} near 590 nm. [26, 28, 44, 46, 52] The red luminescence in this study is considerably broader than usual europium PL due to energy transfer with graphene and functionalities. As shown in Figure 7(a), the PL spectrum was gradually varied as the annealing temperature increased. A peak at 458nm appeared with a decrease in the intensity of the peak at 590nm after annealing at 400 ºC. The peak located at 458nm, which is due to intrashell 4*f*-4*f* transitions with divalent europium, increased dramatically after annealing at 1000 ºC since Eu^{3+} was remarkably reduced to Eu^{2+} by thermally-assisted interaction with carbon and oxygen atoms on graphene sheet. [53, 54] A significant reduction of graphene sheet occurred at 850 ºC, which is the critical temperature where the annealing effect assisted the reaction of europium. [13, 36] State changing from trivalent to divalent europium ions assisted by thermal reduction with graphene sheet contributed to decreasing the emission intensity at 590-600 nm and increasing at 458nm. Furthermore, the bonding

between europium and graphene sheet can produce the defect levels, which generate the lower energy emission peak located at 458 nm than that of thermally reduced graphene oxide (Figure S4), in the band structure of EuG.

In Figure 7(b), 0.05 wt% EuG composed of the smallest europium shows the greatest PL enhancement at 458 nm. Emission intensity can be influenced by the quenching effect, which results from non-radiative energy transfer at high concentration sample. [55, 56] Moreover, with increasing the concentration, the europium coverage change on the graphene surface (Figure 1) effect on the photon energy absorption and decrease in the PL emission intensity, since the europium nanoparticles has lower light absorption characteristics than the graphene sheet. Europium as a metallic chemical element in the lanthanide series provides small absorption at the 258 nm excitation wavelength. Graphene sheet as a main light absorbing platform largely contributes to the excitation. Small number of europium atoms can cover the considerable large area on the graphene surface because europium atom size is about three times larger than carbon and oxygen, europium nanoparticle would be much greater than them in the graphene sheet. The fully annealed composite of the europium and graphene sheet composed of 50 wt% of europium provides the smallest PL enhancement among EuG samples with different concentrations, it revealed higher PL emission intensity than that of the reduced graphene oxide by heat owing to the europium outstanding fluorescent characteristics and the quantum effect of nano-size europium particle (Figure S4).

The quantum yield for 0.05 wt% EuG was calculated with the property of Norharmane, standard material. [57] Using the H_2SO_4 as a solvent, the quantum yield of 0.05 wt% EuG, 0.425 (=42.5%), is extracted from the linearity of integrated fluorescence intensity as a function of absorbance (Figure S5). This efficiency of photoluminescence is higher than that of usual graphene oxide complexes [58] and europium compounds [59] since the graphene sheet

assists to absorb the light and europium composite produce the strong emission. It is similar with nanoparticle studies that plasmonic nanoparticles enhance the absorption of electromagnetic wave and lead the improvement of fluorescence intensity.

Microscope image of black film, which is 0.05 wt% EuG annealed at 1000 °C, is shown in Figure 8(a). In Figures 8(b)-(d), the blue emissions of EuG were observed by fluorescence microscope. Annealed EuG film is black in microscope image, but flakes of EuG show bright fluorescence by UV excitation light. The blue emission at 400 nm of intrinsic 0.05 wt% EuG is described in Figure 8(c) and complex blue emission at 400 and 458 nm, as represented in Figure 8(d), is emitted from annealed EuG at 1000 °C. This wide and high blue fluorescence characteristic arose from EuG, which is different with GO, reduced GO and europium oxide crystal as described in Figure S6. GO and reduced GO provided a small intensity of fluorescence and europium crystal shows bright red emission by UV light of mercury lamp. Annealed EuG flake is smaller than intrinsic EuG flake because EuG flake was shrunk by reduction of oxygenated functionalities during heating.

3. Conclusion

In this paper, we reported the facile synthesis of a graphene based blue fluorescent material by a chemical process and a heat treatment. The improvement in the blue emission at 458 nm and decrease in the red near 590 nm are determined by europium mixed concentration and annealing temperature. The improved photoluminescence can be attributed by the state change of europium from trivalent to divalent and functional groups of graphene sheet supporting the reduction of europium with thermal energy. All these important aspects promote the combination effect of europium and graphene serving as a multifarious booster for the enhancement in the blue emission. Thus, EuG can be considered as a potential candidate for application in the display and optoelectronic device with development of large

area graphene growth and biological sample imaging utilizing a small size of graphene flake. Generally, EuG composite with fluorescent characteristics can be the fascinating material for thin film display due to its atomic thin structure and high blue emission. For the fluorescence imaging of biological samples, the optional adhesion on the target material is significantly important. The functional groups on the EuG can assist the bonding with other molecules and EuG can lead to improvement of the selectivity in the material to observe with appropriate linker. To check the temperature in the high vacuum chamber, which must not allow the internal-external connection for employing thermocouple or probe because tiny leakage lead the critical problem, EuG coated film with tunable fluorescent characteristic according to heat can be utilized as a sensor. Usual non-contact thermometer is designed by using infrared light for detect the thermal energy; otherwise, EuG film temperature sensor uses the state change of material. Under high temperature condition, Infrared imaging of the inside chamber provides the comprehensive information of heat contribution on the several parts such as flow gas, devices, surface of chamber, but, EuG can reveal a specific signal on the localized area with the emission intensity at the fixed wavelength (458 nm).

Acknowledgements

This research was partially supported by the Pioneer Research Center Program (2010-0019313), the National Research Foundation of Korea (NRF) grant funded by the Korea government (MSIP) (NRF-2011-0014219), the Futuristic Fundamental Research Program (2E23831-13-095) funded by Korea Institute of Science and Technology.

References

1. A. H. Castro Neto, F. Guinea, N. M. R. Peres, K. S. Novoselov and A. K. Geim, *Rev. Mod. Phys.*, 2009, 81, 109-162.
2. Y. W. Zhu, S. Murali, W. W. Cai, X. S. Li, J. W. Suk, J. R. Potts and R. S. Ruoff, *Advanced Materials*, 2010, 22, 3906-3924.
3. S. Das Sarma, S. Adam, E. H. Hwang and E. Rossi, *Rev. Mod. Phys.*, 2011, 83, 407-470.
4. H. Kim, A. A. Abdala and C. W. Macosko, *Macromolecules*, 2010, 43, 6515-6530.
5. C. Berger, Z. Song, T. Li, X. Li, A. Y. Ogbazghi, R. Feng, Z. Dai, A. N. Marchenkov, E. H. Conrad and P. N. First, *The Journal of Physical Chemistry B*, 2004, 108, 19912-19916.
6. M. Freitag, *Nature nanotechnology*, 2008, 3, 455-457.
7. H. Raza, *Graphene Nanoelectronics: Metrology, Synthesis, Properties and Applications, NanoScience and Technology*, 2012, 1.
8. F. Bonaccorso, Z. Sun, T. Hasan and A. Ferrari, *Nature Photonics*, 2010, 4, 611-622.
9. G. Eda and M. Chhowalla, *Advanced Materials*, 2010, 22, 2392-2415.
10. S. B. Kulkarni, U. M. Patil, I. Shackery, J. S. Sohn, S. Lee, B. Park and S. C. Jun, *Journal of Materials Chemistry A*, 2013.
11. U. M. Patil, J. S. Sohn, S. B. Kulkarni, H. G. Park, Y. Jung, K. V. Gurav, J. H. Kim and S. C. Jun, *Materials Letters*, 2014.
12. Y. Wang, Z. Shi, Y. Huang, Y. Ma, C. Wang, M. Chen and Y. Chen, *The Journal of Physical Chemistry C*, 2009, 113, 13103-13107.
13. H. M. Ju, S. H. Choi and S. H. Huh, *J. Korean Phys. Soc.*, 2010, 57, 1649-1652.
14. J. Rani, J. Oh, J.-e. Park, J. Lim, B. Park, K. Kim, S.-J. Kim and S. C. Jun, *Nanoscale*, 2013, 5, 5620-5627.
15. Y. Zhang, T.-T. Tang, C. Girit, Z. Hao, M. C. Martin, A. Zettl, M. F. Crommie, Y. R. Shen and F. Wang, *Nature*, 2009, 459, 820-823.
16. A. Chunder, T. Pal, S. I. Khondaker and L. Zhai, *The Journal of Physical Chemistry C*, 2010, 114, 15129-15135.
17. U. Lange, T. Hirsch, V. M. Mirsky and O. S. Wolfbeis, *Electrochimica Acta*, 2011, 56, 3707-3712.
18. G. Williams, B. Seger and P. V. Kamat, *ACS nano*, 2008, 2, 1487-1491.
19. Y. Li, W. Gao, L. Ci, C. Wang and P. M. Ajayan, *Carbon*, 2010, 48, 1124-1130.
20. R. Muszynski, B. Seger and P. V. Kamat, *The Journal of Physical Chemistry C*, 2008, 112, 5263-5266.
21. C. Tan, X. Huang and H. Zhang, *Materials Today*, 2013, 16, 29-36.
22. T. Ramanathan, A. Abdala, S. Stankovich, D. Dikin, M. Herrera-Alonso, R. Piner, D. Adamson, H. Schniepp, X. Chen and R. Ruoff, *Nature Nanotechnology*, 2008, 3, 327-331.
23. H. Bai, C. Li, X. Wang and G. Shi, *Chemical Communications*, 2010, 46, 2376-2378.
24. Y. Li, G. Wang, K. Pan, B. Jiang, C. Tian, W. Zhou and H. Fu, *J. Mater. Chem.*, 2012, 22,

20381-20386.

25. M. da Silva, H. de Jesus Fraga da Costa, E. Triboni, M. Politi and P. Isolani, *J Therm Anal Calorim*, 2012, 107, 257-263.
26. H. Yang, D. Zhang, L. Shi and J. Fang, *Acta materialia*, 2008, 56, 955-967.
27. V. Pol, R. Reisfeld and A. Gedanken, *Chemistry of materials*, 2002, 14, 3920-3924.
28. B. K. Gupta, P. Thanikaivelan, T. N. Narayanan, L. Song, W. Gao, T. Hayashi, A. Leela Mohana Reddy, A. Saha, V. Shanker and M. Endo, *Nano letters*, 2011, 11, 5227-5233.
29. P. Dorenbos, *Journal of Luminescence*, 2003, 104, 239-260.
30. S. H. M. Poort, H. M. Reijnhoudt, H. O. T. vanderKuip and G. Blasse, *J. Alloy. Compd.*, 1996, 241, 75-81.
31. K. Kattel, J. Y. Park, W. Xu, H. G. Kim, E. J. Lee, B. A. Bony, W. C. Heo, Y. Chang, T. J. Kim and J. Y. Do, *Colloids and Surfaces A: Physicochemical and Engineering Aspects*, 2012, 394, 85-91.
32. W. S. Hummers and R. E. Offeman, *Journal of the American Chemical Society*, 1958, 80, 1339-1339.
33. N. I. Kovtyukhova, P. J. Ollivier, B. R. Martin, T. E. Mallouk, S. A. Chizhik, E. V. Buzaneva and A. D. Gorchinskiy, *Chemistry of Materials*, 1999, 11, 771-778.
34. D. Yang, A. Velamakanni, G. Bozoklu, S. Park, M. Stoller, R. D. Piner, S. Stankovich, I. Jung, D. A. Field and C. A. Ventrice Jr, *Carbon*, 2009, 47, 145-152.
35. O. Akhavan, *Carbon*, 2010, 48, 509-519.
36. S. H. Huh, *Physics and Applications of Graphene-Experiments, Nanotechnology and Nanomaterials*, 2011.
37. F. Mercier, C. Alliot, L. Bion, N. Thromat and P. Toulhoat, *Journal of Electron Spectroscopy and Related Phenomena*, 2006, 150, 21-26.
38. A. Lacanilao, G. Wallez, L. Mazerolles, P. Dubot, L. Binet, B. Pavageau, L. Servant, V. Buissette and T. Le Mercier, *Solid State Ionics*, 2013, 253, 32-38.
39. X. L. Tan, X. K. Wang, H. Geckeis and T. Rabung, *Environ. Sci. Technol.*, 2008, 42, 6532-6537.
40. F. Mercier, C. Alliot, L. Bion, N. Thromat and P. Toulhoat, *Journal of electron spectroscopy and related phenomena*, 2006, 150, 21-26.
41. H.-K. Jeong, Y. P. Lee, M. H. Jin, E. S. Kim, J. J. Bae and Y. H. Lee, *Chemical Physics Letters*, 2009, 470, 255-258.
42. S. Some, Y. Kim, Y. Yoon, H. Yoo, S. Lee, Y. Park and H. Lee, *Sci. Rep.*, 2013, 3.
43. T. V. Khai, H. G. Na, D. S. Kwak, Y. J. Kwon, H. Ham, K. B. Shim and H. W. Kim, *J. Mater. Chem.*, 2012, 22, 17992-18003.
44. Z. Mo, Y. Zhao, R. Guo, P. Liu and T. Xie, *Materials and Manufacturing Processes*, 2012, 27, 494-498.
45. T. V. Cuong, V. H. Pham, Q. T. Tran, S. H. Hahn, J. S. Chung, E. W. Shin and E. J. Kim, *Materials letters*, 2010, 64, 399-401.
46. D. D. Wang, H. Gao, E. Roze, K. Qu, W. J. Liu, Y. Shao, S. Y. Xin and Y. Z. Wang, *J. Mater.*

Chem. C, 2013, 1, 5772-5778.

47. S. Gurunathan, J. W. Han, V. Eppakayala and J.-H. Kim, *International journal of nanomedicine*, 2013, 8, 1015.
48. P. Gong, J. Wang, W. Sun, D. Wu, Z. Wang, Z. Fan, H. Wang, X. Han and S. Yang, *Nanoscale*, 2014, 6, 3316-3324.
49. Z. Wang, Y. Li, Q. Jiang, H. Zeng, Z. Ci and L. Sun, *J. Mater. Chem. C*, 2014, 2, 4495-4501.
50. J. Rani, J. Lim, J. Oh, J.-W. Kim, H. S. Shin, J. H. Kim, S. Lee and S. C. Jun, *The Journal of Physical Chemistry C*, 2012, 116, 19010-19017.
51. G. Eda, Y. Y. Lin, C. Mattevi, H. Yamaguchi, H. A. Chen, I. Chen, C. W. Chen and M. Chhowalla, *Advanced Materials*, 2010, 22, 505-509.
52. A. Huignard, V. Buissette, A. C. Franville, T. Gacoin and J. P. Boilot, *J. Phys. Chem. B*, 2003, 107, 6754-6759.
53. J. Hao, J. Gao and M. Cocivera, *Appl. Phys. Lett.*, 2003, 82, 2778-2780.
54. S. Prucnal, J. Sun and W. Skorupa, *Appl. Phys. Lett.*, 2007, 90, 181121-181121.
55. J. Sun, W. Skorupa, T. Dekorsy, M. Helm, L. Rebohle and T. Gebel, *J. Appl. Phys.*, 2005, 97, 123513.
56. E. Moretti, A. Talon, L. Storaro, A. Le Donne, S. Binetti, A. Benedetti and S. Polizzi, *Journal of Luminescence*, 2014, 146, 178-185.
57. A. Pardo, D. Reyman, J. M. L. Poyato and F. Medina, *Journal of Luminescence*, 1992, 51, 269-274.
58. Q. Mei, K. Zhang, G. Guan, B. Liu, S. Wang and Z. Zhang, *Chemical Communications*, 2010, 46, 7319-7321.
59. N. B. D. Lima, S. M. C. Goncalves, S. A. Junior and A. M. Simas, *Sci. Rep.*, 2013, 3.

Figure captions

Figure 1: TEM images and scaled-up views of EuG samples with (a) 0.05 wt%, (b) 0.5 wt%, (c) 1 wt% and (d) 50 wt% of europium concentration. (Inset images in (a), (b) are selected area electron diffraction (SAED) patterns)

Figure 2: XPS spectra of (a)-(d) C1s and (e)-(h) Eu3d orbitals of intrinsic EuG composite and annealed samples from 400 ºC to 1000 ºC with different concentrations of europium: (a) and (e) correspond to 0.05 wt%, (b) and (f) to 0.5 wt%, (c) and (g) to 1 wt%, and (d) and (h) to 50 wt%.

Figure 3: XRD pattern from EuG samples with different europium concentrations and annealing temperatures: (a) 0.05 wt%, (b) 0.5 wt%, (c) 1 wt%, and (d) 50 wt% EuG annealed from 400 ºC to 1000 ºC.

Figure 4: (a)-(d) Raman shifts spectra of EuG samples with different europium concentrations and annealing temperatures, (e)-(h) I_D/I_G ratios and (i)-(l) FWHM of G and D bands. (a), (e), and (i) correspond to 0.05 wt%; (b), (f) and (j) to 0.5 wt%; (c), (g), and (k) to 1 wt% and (d), (h), and (l) to 50 wt%.

Figure 5: FT-IR spectra of (a) 0.05 wt%, (b) 0.5 wt%, (c) 1 wt% and (d) 50 wt% EuG with different temperatures from 400 to 1000 °C

Figure 6: Absorbance spectra of EuG samples, 0.05 to 50 wt% with different annealing temperatures from 400 to 1000 ℃.

Figure 7: PL features after annealing as a function of annealing temperature and europium concentration: (a) PL emission of 0.05 wt% EuG with different annealing temperatures from room temperature to 1000 ºC, (b) PL emission annealed at 1000 ºC with different europium

concentrations from 0.05 wt% to 50 wt%.

Figure 8: Optical microscope and fluorescence microscope image of EuG 0.05 wt% excited by UV light of mercury lamp: (a) Optical microscope image, (b) Fluorescence microscope image of full annealed 0.05 wt% EuG and scale up views of fluorescence images of (c) intrinsic and (d) full annealed 0.05 wt% EuG flake.

Supplementary Information

Figure S1. : TEM image and scaled-up views of ultrasmall europium oxide nanoparticles.

Figure S2. : (a)-(d) O1s XPS spectra of intrinsic EuG composite and annealed samples at 1000 ºC with different concentrations of europium: (a) correspond to 0.05 wt%, (b) to 0.5 wt%, (c) to 1 wt%, and (d) to 50 wt%.

Figure S3. : At 458 nm emission, photoluminescence excitation spectra of (a) 0.05 wt%, (b) 0.5 wt%, (c) 1 wt% and 50 wt% EuG with different temperatures from 400 to 1000 °C.

Figure S4. : Photoluminescence emission spectrum of reduced graphene oxide, europium decorated graphene (50 wt% of europium) both of samples annealed until 1000 °C.

Figure S5. : Linear plots of integrated fluorescence intensity *vs*. absorbance and the equation for achievement of quantum yield with 0.05 wt% annealed EuG and Norharmane ($\Phi = 0.51$). Φ is the photoluminescence quantum yield, *Grad* is the gradient from the plot of integrated fluorescence intensity as a function of absorbance. n is the refractive index of the solvent containing sample.

Figure S6. : (a)-(c) Microscope and (d)-(f) fluorescence images with mercury UV lamp: (a)

and (d) correspond to GO, (b) and (e) to reduced GO, (c) and (f) to europium oxide crystal.

Figure 1.

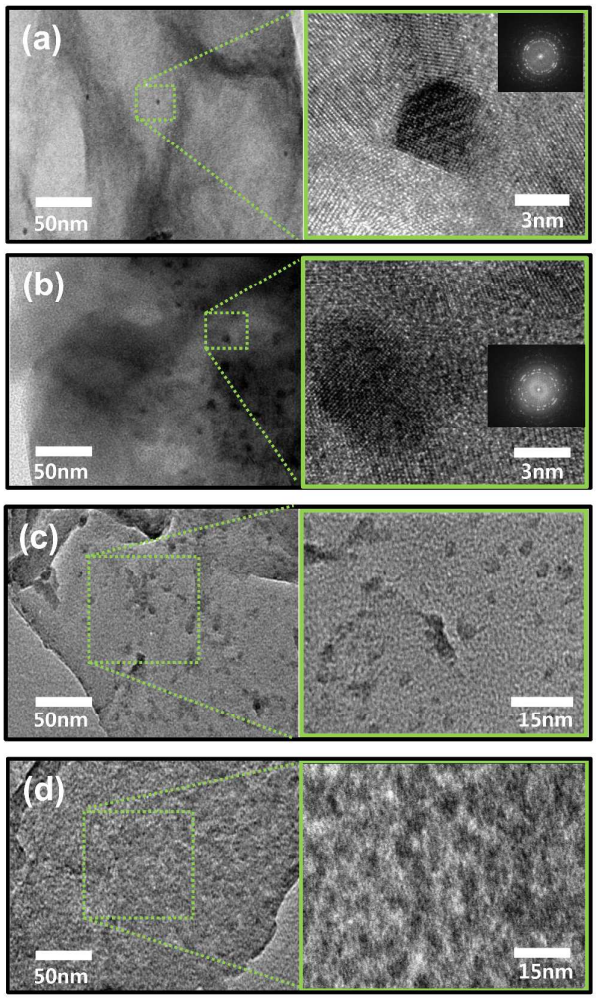

Figure 2.

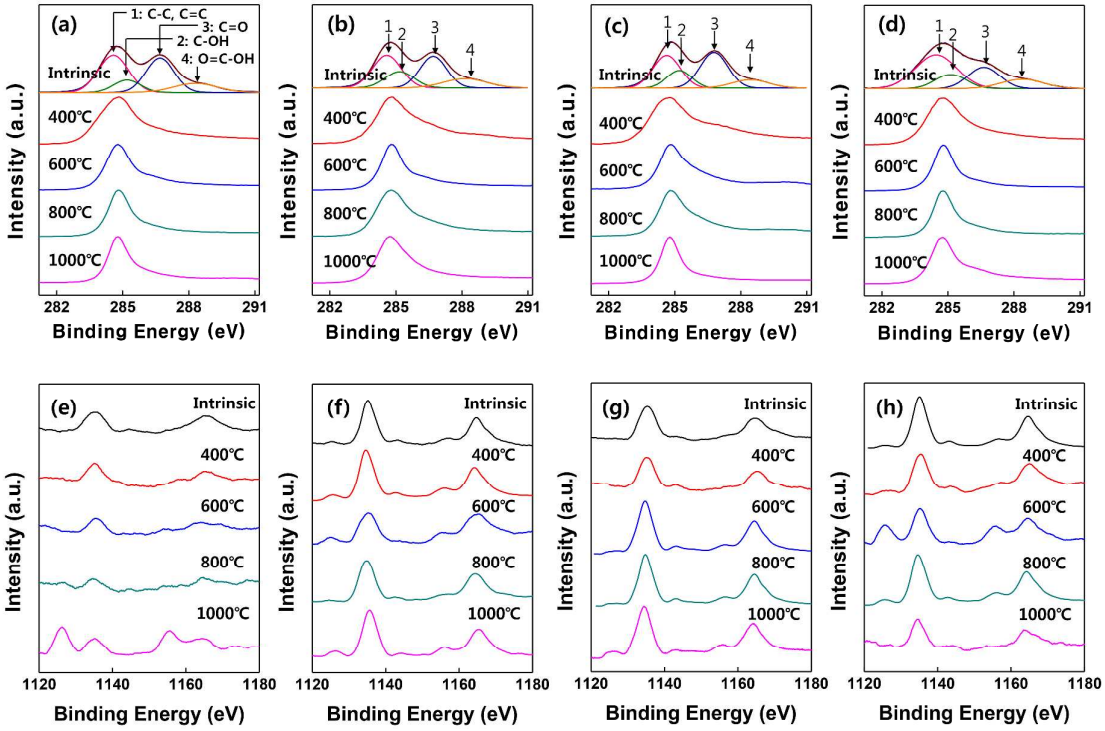

Figure 3.

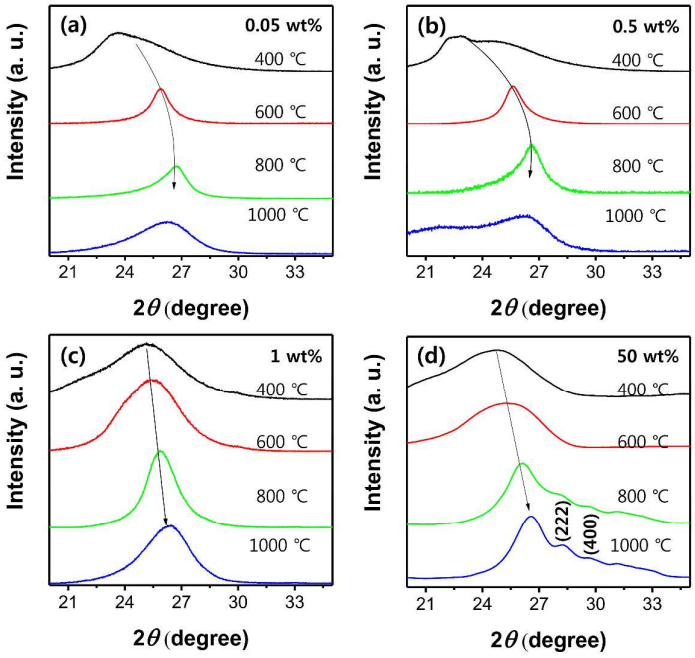

Figure 4.

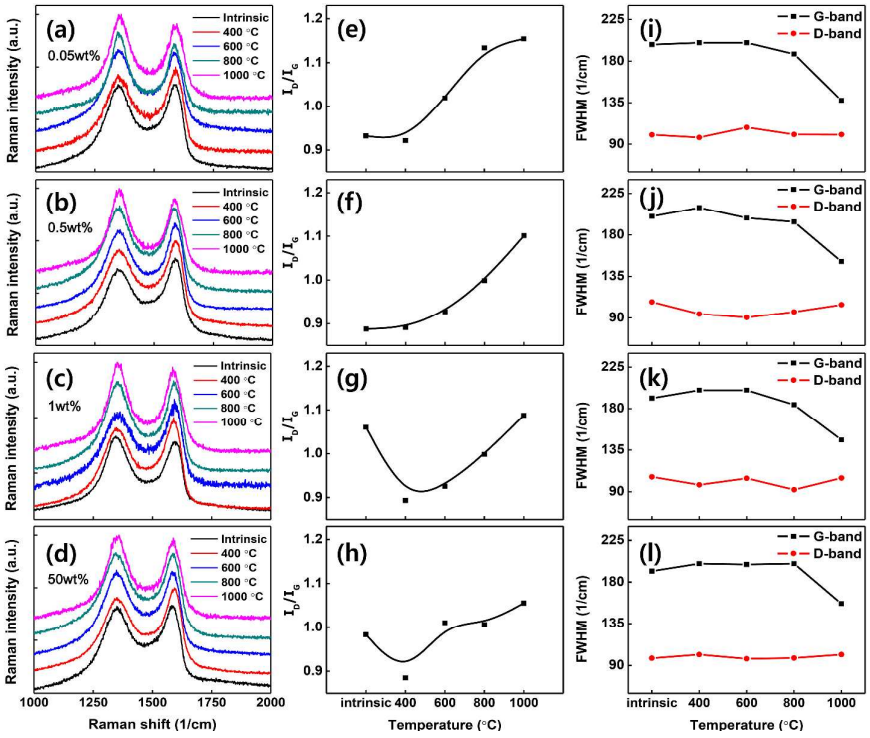

Figure 5.

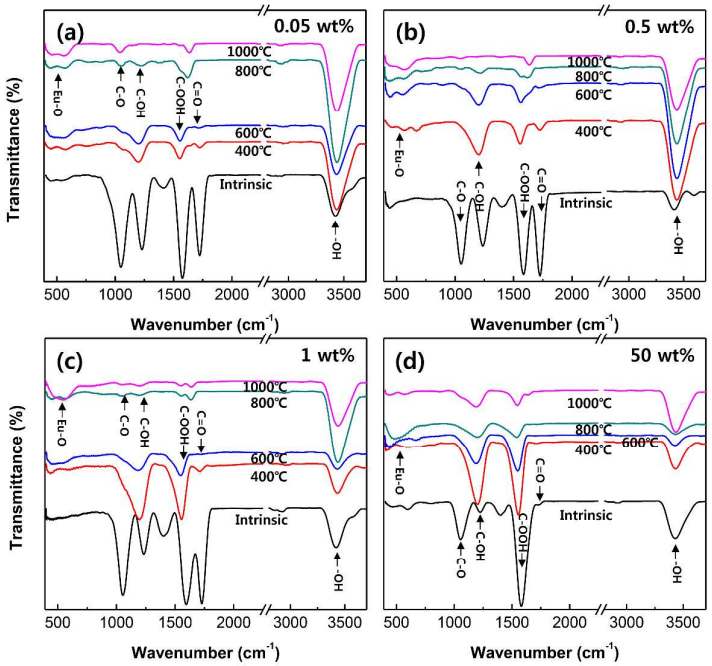

Figure 6.

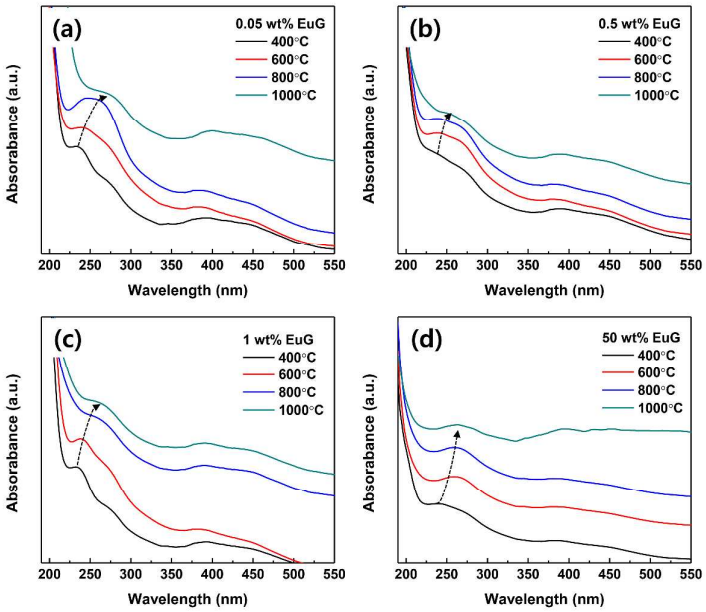

Figure 7.

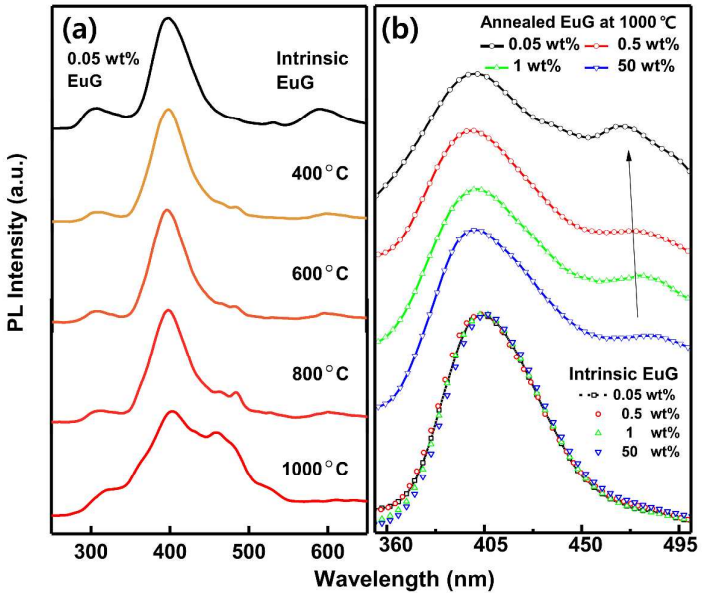

Figure 8.

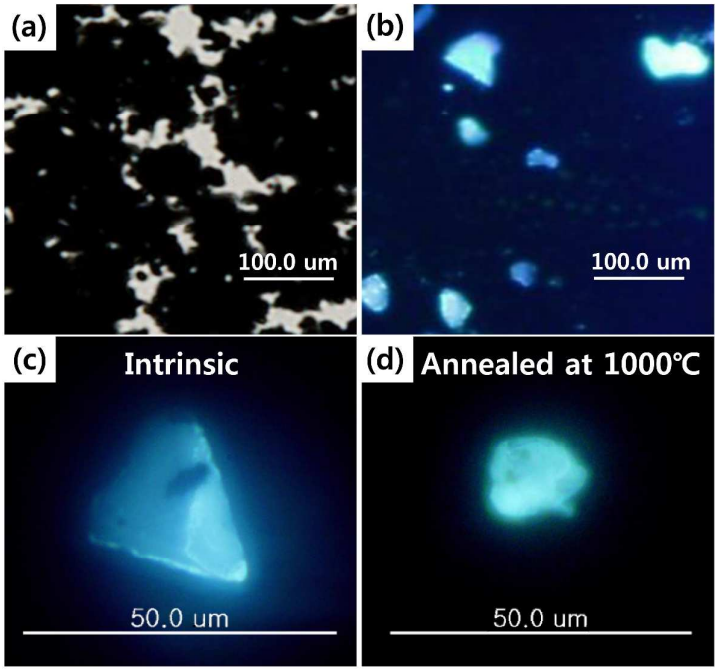

Graphical Table of Contents

: Europium decorated graphene provides photoluminescence feature change with enhancement of blue emission located at 458 nm after thermal reduction.